Post-Earthquake Forensic Examination of Two Unreinforced Masonry Buildings via Discontinuum-Based Analysis

Andrei FARCASIU[1]
Peter GRIESBACH[2]
Rhea WILSON[3]
Sinan ACIKGOZ[4]
Bora PULATSU[5*]

ABSTRACT

Post-earthquake investigations show that unreinforced masonry (URM) buildings may exhibit diverse failure mechanisms depending on the construction morphology and the connection detailing between their structural components. Advanced computational models are necessary to consider the influence of these aspects. However, realistically reproducing the post-collapse state of an existing URM building is challenging when limited data is available on the aforementioned features. To address this challenge, a framework for exploring the seismic behavior of URM buildings is presented. The current investigation presents two case study buildings located in Türkiye's Hatay province: the Mithatpaşa Primary School in Iskenderun and the Liwan Boutique Hotel in Antakya, both of which suffered partial collapses during the recent Kahramanmaraş Earthquakes in 2023. Discrete block models of the two case study buildings are generated based on geometrical information obtained from various pre- and post-collapse vision-based data sources. An automatic block generation algorithm is proposed to replicate periodic and nonperiodic masonry wall patterns. Next, the generated discrete block media are analyzed using discontinuum-based structural analysis to predict the seismic response of the structures. Comparisons between the

Note:

- This paper was received on October 12, 2024 and accepted for publication by the Editorial Board on April 16, 2025.
- Discussions on this paper will be accepted by November 30, 2025.

- https://doi.org/10.18400/tjce.1565654

1 Carleton University, Civil and Environmental Engineering Department, Ottawa, Canada
andreifarcasiu@cmail.carleton.ca - https://orcid.org/0009-0002-3692-1840

2 Carleton University, Civil and Environmental Engineering Department, Ottawa, Canada
petergriesbach@cmail.carleton.ca - https://orcid.org/0009-0007-3552-9018

3 Carleton University, Civil and Environmental Engineering Department, Ottawa, Canada
rheaswilson@cmail.carleton.ca - https://orcid.org/0000-0003-1171-2110

4 University of Oxford, Department of Engineering Science, Oxford, United Kingdom
sinan.acikgoz@eng.ox.ac.uk - https://orcid.org/0000-0002-3901-574X

5 Carleton University, Civil and Environmental Engineering Department, Ottawa, Canada
bora.pulatsu@carleton.ca - https://orcid.org/0000-0002-7040-0734

* Corresponding author

preliminary pushover analysis results and collapse observations inform further analyses, and lead to an exploration of how construction morphology and connection detailing may have contributed to the partial collapse of the buildings. It is demonstrated that this iterative approach, supported by forensic site evidence and reverse engineering analysis, provides new insight into the influence of key factors that contribute to collapse. This information can help safeguard similar structures and inform the development of effective retrofitting solutions.

Keywords: Masonry, computational modeling, structural analysis, discrete element method, collapse mechanism, forensic engineering.

1. INTRODUCTION

Predicting the seismic behavior of unreinforced masonry (URM) buildings is a complex task. Ideally, the adopted numerical models should predict the maximum lateral load carrying capacity of the URM structure, as well as the associated progressive damage and collapse mechanisms. The frequently used structural analysis techniques are performed via computational models based on finite and/or discrete element methods [1]. Continuum-based models treat masonry as a homogenous medium without distinguishing between masonry units or mortar joints (*e.g.*, [2–5]). On the other hand, discontinuum-based models explicitly represent masonry constituents with different levels of complexity (*e.g.*, [6–10]).

In the last two decades, discontinuum-based analysis of URM structures has become increasingly popular [11]. In particular, the discrete element method (DEM) has been extensively used to explore the mechanics of URM walls, arches, and buildings. DEM is ideally suited for high-fidelity post-earthquake forensic examination of URM buildings as it facilitates the consideration of wall morphology and connection detailing. Since the accuracy of discontinuum-based analyses specifically depends on how precisely the geometrical and morphological features are implemented in the computational model, special attention should be given to the idealization of block geometries in the discontinuum-based computational models. Within this context, 3D models of URM buildings informed via LiDAR scans or photogrammetry often serve as the basis of block size and other features related to wall construction quality [12–15]. The actual block geometry is frequently simplified via manual or semi-automatic procedures when developing discrete block models to minimize computational model run times.

While discontinuum-based analysis offers promising features regarding collapse simulations, its potential use in testing various structural configurations to reproduce different collapse mechanisms has not been systematically investigated in the literature. This is especially the case in the context of post-earthquake forensic investigations. Therefore, the present research aims to demonstrate an innovative application of discontinuum-based analysis of two masonry buildings that suffered partial collapses after the recent Kahramanmaraş Earthquakes (2023). One novel aspect of this research lies in the automatic generation of discontinuum-based models using pre- or post-collapse visual records of URM buildings. The proposed iterative use of computational models reproduces various collapse mechanisms of the buildings, enabling discontinuum-based analyses in the reverse engineering approach. Hence, different what-if scenarios are examined to understand the impact of various poorly characterized but critical aspects on the response of the URM buildings.

The analyzed URM buildings are shown in Figure 1: the Mithatpaşa Primary School in Iskenderun and the Liwan Boutique Hotel in Antakya. These buildings are both from the early 20th century, built during the French Mandate period of Hatay. A contemporary poster describing an inscription on the building suggests that the Mithatpaşa Primary School in Iskenderun was constructed originally as a hospice. Research [16] also indicates that the building may have been used as a school for nuns before its conversion to a secular primary school after 1939. The school is comprised of two buildings; only the annex building, which got damaged, will be investigated in this study. The first storey of the building is dedicated to classrooms separated by internal walls, while the second storey serves as a single unpartitioned conference room. This part of the structure collapsed during the earthquake. The second investigated structure, Liwan Hotel, was built as the home of Suphi Bereket, the first president of the Syrian Federation during the French Mandate. The building also served as an administrative centre of the Federation. The use of the building as a hotel is recent and dates back to 2008. The front façade of the building collapsed during the Kahramanmaraş earthquakes.

(a) *(b)*

Figure 1 - Post-earthquake conditions of the analyzed URM buildings: (a) Mithatpaşa Primary School, Iskenderun, and (b) Liwan Boutique Hotel, Antakya.

The paper is organized as follows. Section 2 presents the adopted DEM modeling strategy. The proposed discrete block representation of the analyzed URM buildings is discussed in Section 3, and the results of the discontinuum-based nonlinear analyses under quasi-static loading are provided in Section 4. Finally, important inferences are discussed, and conclusions are drawn in Section 5.

2. ADOPTED DISCONTINUUM-BASED COMPUTATIONAL MODELING STRATEGY

The seismic response of two URM buildings is investigated via DEM, pioneered by Cundall [17]. This approach captures the nonlinear behavior of masonry by representing it as a system of discrete blocks interacting with each other at contact points [18, 19]. The simplified micro-modeling approach is used where the masonry units are expanded up to the half-thickness of the mortar joints, as shown in Figure 2. In this idealization, the masonry units can be modeled as rigid or deformable blocks, while the unit-mortar interface (bond) is considered at the zero-thickness interface [20, 21].

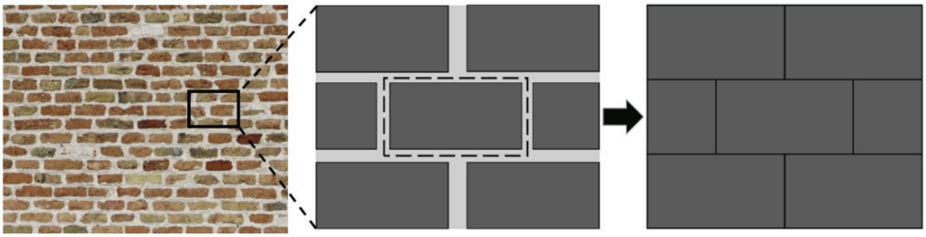

Figure 2 - Illustration of generated discrete block medium based on the simplified micro-modeling approach.

The present study relies on the strong unit weak mortar assumption; hence, rigid blocks are utilized to model the full-scale URM buildings in 3DEC (three-dimensional discrete element code – a commercial software developed by Itasca Consulting Group [22]). The rigid block movements are calculated by solving the governing equations of motion using the central difference method to predict translational and rotational velocities, presented in Equations (1) and (2), respectively.

$$\dot{u}_i^{t+} = \dot{u}_i^{t-} + \frac{\Delta t}{m}(\Sigma F_i^t - \lambda|\Sigma F_i^t| sgn(\dot{u}_i^{t-})) \tag{1}$$

$$\omega_i^{t+} = \omega_i^{t-} + \frac{\Delta t}{I}(\Sigma M_i^t - \lambda|M_i^t| sgn(\omega_i^{t-})) \tag{2}$$

where $\dot{u}_i$ and ω_i are the translational and rotational velocities of the block centroid, respectively. The sum of forces and moments acting on a block is obtained via ΣF_i^t and ΣM_i^t, denoted as unbalanced force and moment. Additionally, m, I and Δt indicate the block mass, the moment of inertia, and the time step. Note that the formulation calculates block velocity at the mid-time step (*i.e.*, $t^+ = t + \Delta t/2$; $t^- = t - \Delta t/2$). To prevent numerical instability, the critical time step (Δt_c) is calculated in terms of the minimum block mass (m_{min}) and the maximum contact stiffness ($k_{n,max}$) in the system ($\Delta t_c = \sqrt{m_{min}/k_{n,max}}$). Cundall's local damping formulation ($F_d = \lambda|F_i^t| sgn(\dot{u}^{t-})$, $M_d = \lambda|\Sigma M_i^t| sgn(\omega^{t-})$) is applied to obtain quasi-static solutions, providing a damping force opposing motion proportional to the local unbalanced force [23]. The adopted damping scheme uses a non-dimensional damping constant (λ), which has a default value of 0.8.

Contact constitutive laws govern the interaction between discrete blocks in DEM. When two blocks get into contact, a series sub-contacts are generated along the contacting surfaces. At each sub-contact, three orthogonal springs are defined: one in the normal direction and two in the shear direction. The present study adopts a soft contact approach, allowing blocks to overlap according to their contact stiffnesses in the normal and shear directions (k_n and k_s, respectively). Once the position of each rigid block is updated by integrating the predicted velocity, the relative point contact displacement increments for the adjacent blocks in the normal (Δu_n) and shear ($\Delta u_{s,i}$) directions are calculated. Then, elastic normal ($\Delta\sigma$) and shear ($\Delta\tau_{s,i}$) contact stress increments are obtained as follows.

$$\Delta\sigma = k_n \Delta u_n;\ \Delta\tau_{s,i} = k_s \Delta u_{s,i} \tag{3}$$

New contact stresses are calculated by adding the stress increments to the contact stresses from the previous time step ($\sigma^{t+} = \Delta\sigma + \sigma^t$, $\tau_{s,i}^{t+} = \Delta\tau_{s,i} + \tau_{s,i}^t$) and corrected according to the defined failure criterion (if applicable). A contact stress update routine is executed within the explicit solution scheme of the DEM. The present research utilizes a simple elasto-brittle contact model (characterised by tensile strength f_T) to capture the weak bond behavior. In shear, the Coulomb-slip Joint model is adopted, where the bond cohesion (c) and friction angle (ϕ) are used to calculate the shear strength (τ), while the residual shear capacity (τ_{res}) is controlled by the residual cohesion (c_{res}), and residual friction angle (ϕ_{res}). The assigned contact stress-displacement behavior in tension, compression, and shear regimes are illustrated in Figure 2.

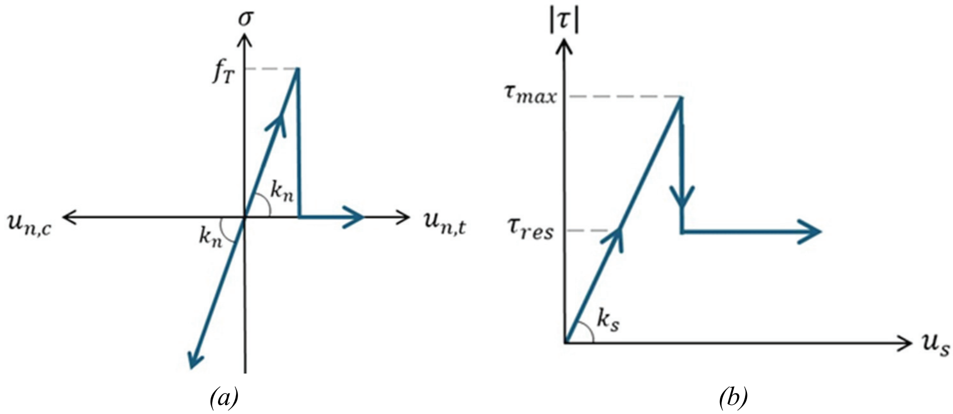

Figure 3 - Defined elasto-brittle contact models in the normal (a) and shear (b) direction.

Finally, the updated contact stresses are multiplied by the associated sub-contact area and utilized in the equations of motion. The explicit solution procedure continues until a quasi-static solution or a defined displacement limit is reached during the analysis. Nonlinear pushover analysis is performed following the procedures discussed above to predict the seismic response of the two URM buildings.

3. DISCRETE BLOCK REPRESENTATION OF URM BUILDINGS

Different workflows are proposed in the literature to utilize vision-based data to generate computational models [24–27]. In this research, a practical approach is employed, where a data-driven automated block generation algorithm is implemented. The adopted strategy can generate periodic and nonperiodic masonry patterns, allowing for flexibility in representing various construction typologies. Nonperiodic patterns are categorized into patterns with and without horizontal courses; the latter type is referred to as rubble masonry. The measurements used to generate the DEM-based models are obtained from post-collapse laser scans, predisaster visual records, GIS data, and 360 photography from Google Maps. As such, the accuracy in geometric representation of the buildings varies depending on the available data.

3.1. Determination of Overall Building Geometry

The geometrical properties of the Mithatpaşa building are determined from recently acquired laser scan point cloud data [28]. This technology captures detailed spatial information by measuring the phase shifts or time of arrival of reflected light produced by infrared laser beams. The spatial information from the laser scans is used to determine the plan dimensions of the building, the thickness of the walls (*i.e.*, 0.5 m), and the characteristic dimensions of the masonry units. Since the buildings were scanned after the earthquakes, the window locations on the collapsed second-floor walls are extrapolated based on the sizes and spacing of openings on the first floor. These assumptions are qualitatively verified using pre-collapse photographs in the literature [16].

In contrast, point cloud data is not available for the Liwan Hotel. Instead, its geometrical properties are estimated using lower-accuracy GIS data and 360 panoramic images from Google Maps. To obtain an orthographic view of the building entrance elevation, an image from Google Street View is corrected using Adobe Photoshop's "*perspective warp*" tool. This corrected image is later used to estimate key dimensions, including the overall building height, the locations and sizes of window and door openings, and the characteristic dimensions of masonry units [29]. Additionally, GIS data is used to approximate the building's plan dimensions. Due to the lack of direct measurements, the wall thickness is estimated as 0.75 meters based on collapse photographs and comparisons with similar buildings in the area.

Once the general dimensional measurements for both buildings are obtained, they are used to create simplified CAD drawings. Next, the obtained 3D CAD drawings are utilized by the automatic block generation algorithm, discussed in the next section. This workflow is summarized in Figure 4.

3.2. Generation of Periodic Block Geometry

Using the dimensions extracted from the CAD files, an automated pipeline is implemented in Python to create discrete block models of URM walls for discontinuum-based analysis. The process begins by subdividing the 3D solid envelopes of the URM walls into evenly spaced grids, which are then populated with blocks arranged in a regular running bond pattern.

While the characteristic dimensions of the masonry units are estimated in Section 3.1, block-based representation of the analyzed unreinforced masonry buildings at a 1:1 scale is computationally prohibitive. Relatively few examples exist in the literature incorporating a large number of blocks in DEM-based simulations [9, 30]. In this study, the block size is increased to optimize efficiency in both the Mithatpaşa Building and the Liwan Boutique Hotel. However, caution is necessary, as excessive upscaling may reduce the accuracy of the crack pattern and unrealistically increase the predicted structural capacity. The unit size is chosen to capture the overall macro-behavior of the structures while maintaining model efficiency.

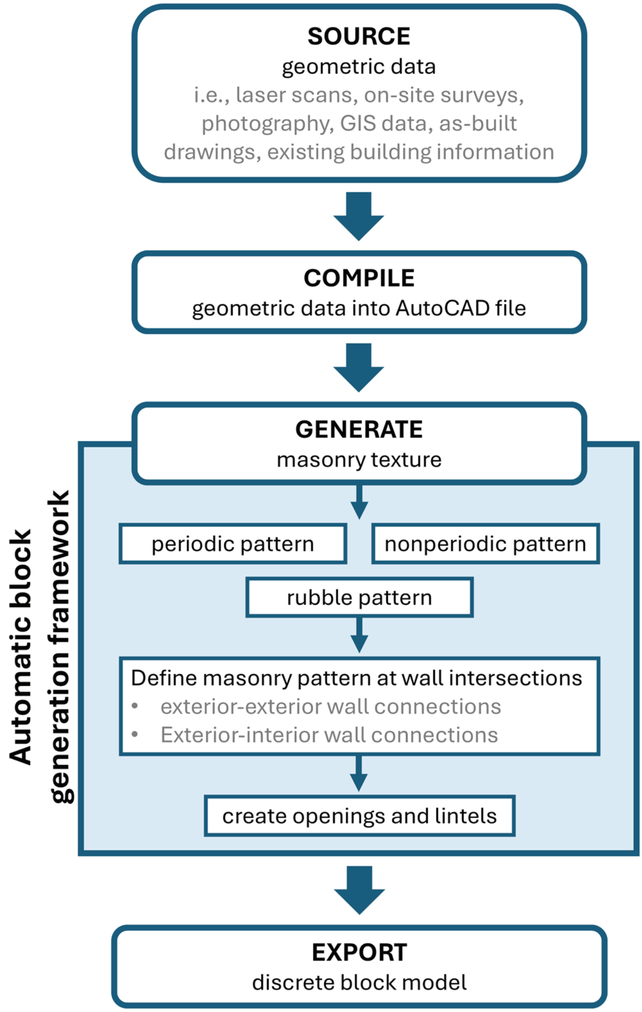

Figure 4 - Proposed framework for generating discrete block URM buildings.

In the absence of further details, the block-generation algorithm assumes well-connected walls with staggered joints at the corners. At exterior and interior-exterior wall intersections, it applies a consistent interlocking pattern to facilitate force transfer between load-bearing walls (Figure 5a-b).

Once the walls and their connections are generated, the openings and lintels are defined based on the available geometric data. To avoid the formation of unnecessarily small blocks that increase computational cost, openings are aligned with bed and head joints, ensuring that only full and half masonry units are used. Finally, the grid coordinates are converted into numerical data for integration into the DEM-based modeling framework.

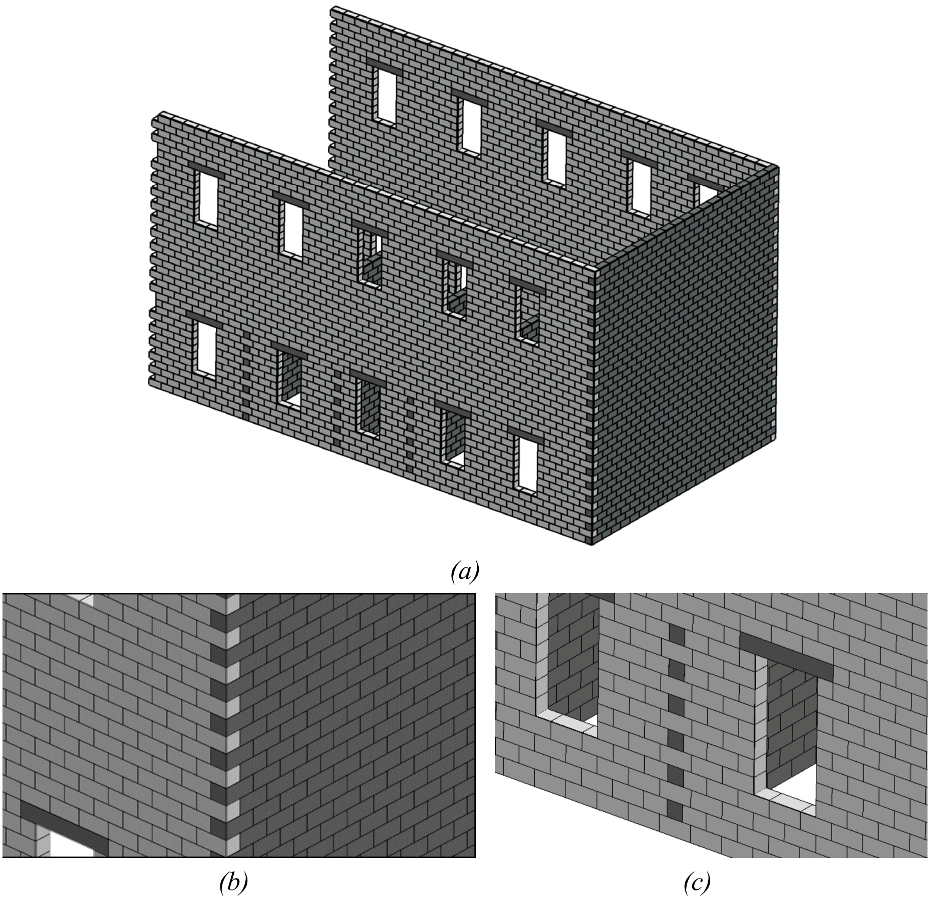

Figure 5. Automatically generated periodic masonry pattern: (a) overall URM structure, (b) staggered joint at corners, and (c) interface between interior and exterior walls.

3.3. Generation of Nonperiodic Block Geometry with Horizontal Courses

The algorithm outlined in the previous section efficiently generates discrete block models with regular running bond. However, masonry patterns are not always regular, and nonperiodic arrangements must also be considered to accurately capture structural behavior. This is particularly important in regions such as Hatay, where stone masonry buildings are often characterized by horizontal courses but with nonperiodic bond patterns. Therefore, an alternative block-generation strategy is introduced to account for these wall morphologies.

The proposed approach for generating nonperiodic masonry patterns begins with selecting a representative section of an existing URM wall (if applicable) or defining a hypothetical wall section. The block size distribution and the horizontal offset of the head joints are measured and used to statistically generate blocks that fill a given volume while maintaining the morphological characteristics of the representative section. Block size distribution can be obtained automatically using advanced pattern recognition algorithms (e.g., [31]) or determined manually. When actual wall cross-section properties are unavailable, a synthetic block size distribution can be used. The horizontal offset of head joints is measured using the M_l ratio, a non-dimensional parameter representing the ratio between the least possible distance passing through mortar joints and the straight distance between the two points (see Figure 6a). This metric is part of the Masonry Quality Index (MQI) introduced by Borri et al. [32, 33].

It should be noted that the M_l ratio may not necessarily be constant in a given wall. A sample distribution of M_l values measured from multiple walls, along with example measurements, are presented in Figure 6b. In nonperiodic masonry constructions, measuring the M_l ratio along different mortar joint paths from top to bottom within a single wall rarely yields identical values (Figure 6c). A similar variation is observed in the nonperiodic discrete block patterns generated using the proposed approach.

The block selection procedure follows a structured approach, constructing the wall row by row and filling each row from left to right. In the first row, block sizes are selected randomly according to the predefined block size distribution. Once the first row is placed, a similar selection strategy is applied; however, instead of randomly selecting a block, multiple candidates are considered for each position. Among these candidates, the block that maximizes the offset from head joints in the adjacent completed row is chosen for placement. An automatic calibration tool determines the number of candidates evaluated during selection, which generates different wall configurations for varying candidate sample sizes and measures the resulting M_l ratio. The candidate sample size that best approximates the expected M_l ratio observed in the wall sample is used. In some cases, none of the candidates yields an M_l ratio low enough to match the defined wall sample. As a result, the block selection strategy can be adjusted to minimize rather than maximize the vertical offset between head joints with the previous row.

Table 1 - Implemented nonperiodic wall generation algorithm (pseudo-code).

Input: *R* (current row), *S* (set of sample blocks), *C* (candidate size), *W* (actual or synthetic wall geometry)
Output: *B* (new block to be added into wall geometry)
If *R* = 1: *// First row is generated without consideration for head joint offset*
    B = randomly selected block from *S*
Else if *R* != 1: *// All other rows are generated based on head joint offset*
    S = {}
    For *i* in 1 to *C*: *// Create set of candidate blocks of size C*
        $B_{Candidate,i}$ = randomly selected block from *S*
        $B_{Candidate,i,OS}$ = distance from the nearest head joint in the adjacent row of *W* to the potential head joint on the right of $B_{Candidate,i}$ *// Referred to as block offset score*
        Add $B_{Candidate,i}$ to *S*
    End For
    B = $B_{Candidate,i}$ within *S* with lowest associated $B_{Candidate.i,OS}$ *// The highest $B_{Candidate.i,OS}$ value can instead be selected to create very low M_l ratio walls.*
End if
B is added to *W*

The adopted pseudo-code for nonperiodic wall block generation is outlined in Table 1, detailing the procedure for selecting the next block. This process is repeated for the leftmost unoccupied space in each row until the row is filled, with subsequent rows following the same approach until the wall is fully constructed.

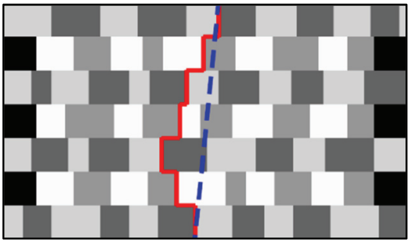

(a)

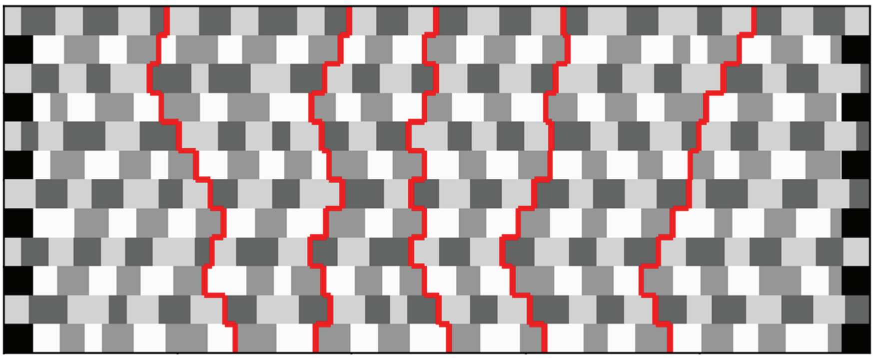

(b)

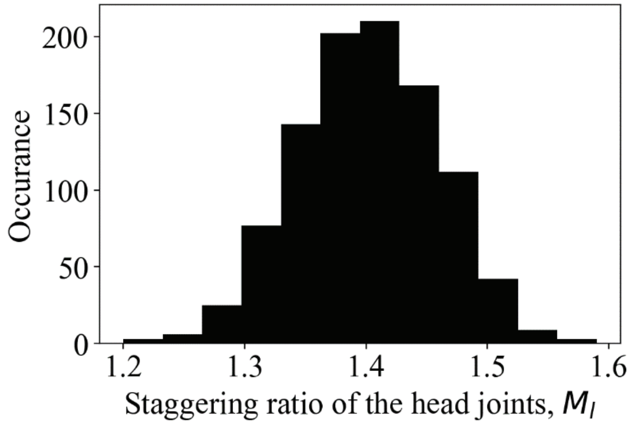

(c)

Figure 6 - (a) Computation of the M_l ratio: Stepped line (red) top to bottom divided by the straight line (blue), (b) illustration of various paths for computing M_l, and (c) a typical M_l distribution of a virtually generated URM wall section.

3.4. Generation of Nonperiodic Block Geometry without Horizontal Courses ('Rubble')

While the nonperiodic masonry generator described in the previous section considers the variability in block size, it does not fully capture rubble geometry. Rubble masonry walls exhibit irregular block shapes and variable joint thicknesses, resulting in non-horizontal courses. To address these complexities, a simple rubble masonry generation method is introduced, allowing for the representation of irregular stone arrangements and improving the accuracy of structural assessments. Irregular (rubble) masonry patterns are generated using an in-house triangular block generator, which allows control over pattern regularity and block size distribution [34]. The process begins by subdividing each wall into a regularly spaced two-dimensional grid. Seed points are placed at the centroid of each grid cell and then randomly shifted based on a user-defined randomness parameter, creating an irregular tessellation while minimizing planar alignment between blocks. Once the seed points are generated for each wall, a MATLAB-based Delaunay triangulation script constructs a two-dimensional mesh, which is then extruded through each wall thickness to form the 3D discrete block geometry.

Wall connection detailing is modeled by joining neighboring tetrahedral shapes at the corners, leading to corner detailing with staggered joints. Similarly, to achieve a preliminary representation of the irregular shape and size variations, triangular prism blocks are randomly joined to form larger polyhedral units, resulting in an unstructured tessellation. Additionally, lintels are incorporated based on dimensions extracted from the CAD drawing.

4. PUSHOVER ANALYSIS AND THE PROPOSED REVERSE ENGINEERING FRAMEWORK

Discrete block models of the two case study buildings, Mithatpaşa and Liwan Hotel, are generated following the automatic generation procedures outlined in the previous section (see Figure 7a and b, respectively). A regular masonry pattern is adopted for the Mithatpaşa case study based on the available on-site information. In contrast, less information is available for the Liwan Hotel masonry pattern, leading to the generation of three different morphologies. Then, discrete block models are used to conduct nonlinear quasi-static (pushover) seismic analysis. Several analyses are applied to assess the influence of various aspects on the failure mechanisms of the buildings.

A density of 2000 kg/m^3 is used for rigid blocks in all discrete element models. The elastic and plastic contact properties are determined in line with similar studies published in the literature (*e.g.*, [35–37]). The contact stiffness in the normal and shear directions is defined as 10^9 Pa/m and 0.4×10^9 Pa/m, respectively. Moreover, the initial and residual friction angles are assumed to be 37 degrees. According to post-earthquake failure observations and non-destructive material tests, poor quality mortar joints were common in the historic buildings of the Hatay province [28]. To represent this, either dry joints are assumed (*i.e.*, $f_T = 0$ and $c = 0$, Mithatpaşa Building) or a limited bond strength is considered (*i.e.*, $f_T = 0.1$ MPa and $c = 0.2$ MPa, Liwan Boutique Hotel). The boundary conditions of the models were established by restricting the bottom course of masonry from displacing and rotating in all degrees of freedom. Once each computational model is brought into equilibrium under its self-weight, lateral accelerations (constant at any one instant) are applied gradually in an incremental fashion along the longitudinal or transversal axis of the building. During the analysis, several monitoring points are utilized to record displacements through the height of the buildings and determine the initial kinematic mechanism. Overall convergence conditions and automatic lateral load increments are programmed in FISH language (an executable programming language in 3DEC).

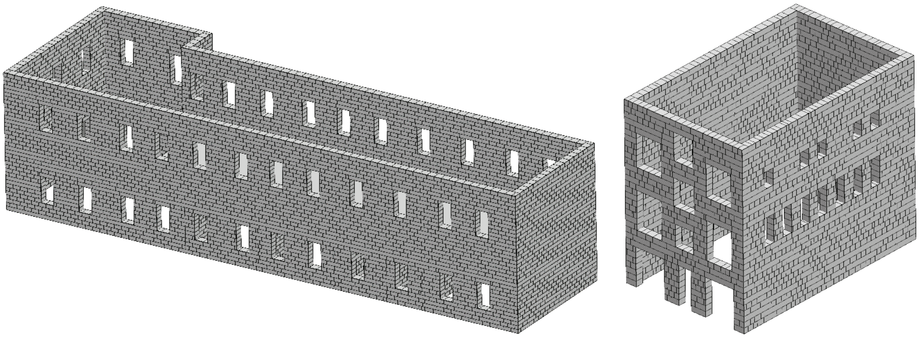

(a) *(b)*

Figure 7 - Discrete block representation of analyzed buildings: (a) Mithatpaşa Primary School, (b) Liwan Boutique Hotel.

4.1. Building #1: Mithatpaşa Building

Four structural configurations are considered for the Mithatpaşa Building, as shown in Figure 8. The first iteration (Figure 8a) includes only the exterior façade of the building, while the second one (Figure 8b) consists of five interior walls, well connected with the exterior envelope. In other models, the diaphragm action is considered by adding continuous rigid bond beams (see Figure 8c) or a floor slab (Figure 8d). The investigation of different configurations is necessary due to the uncertainties associated with the floor structures. Visual evidence suggests the use of a jack arch floor for the main building, while the stairs and floor structures in the extruded part may have been later additions, constructed of reinforced concrete. No structural cracks were observed in the extruded portion of the building during the post-earthquake on-site investigations. Lateral accelerations were applied along the transversal direction of the building.

The failure mechanisms and the associated maximum accelerations are given in Figures 9 and 10, respectively. Results indicate a combined out-of-plane arching action with the overturning mechanism of the façade along the entire wall length when the interior walls are neglected (*Config#1*, Figure 9a). While this mechanism is likely to occur if there is no proper diaphragm action, the extruded portion of the building demonstrated almost no damage, as mentioned earlier. The lack of damage is attributed to the retrofitted stair and floor structure in this section of the building. Hence, the boundary conditions are updated, and in the second structural configuration, the extruded portion of the building is fixed in place, denoted as *Config#2*. The performed update yields a local overturning failure at the second storey, as shown in Figure 9b. The following iterations introduce five interior walls along the ground floor. Both simulations are executed without and with the extruded section fixed. The former

(*Config#3*) leads to a failure mechanism along the entire length of the second storey (Figure 9c), while the latter (*Config#4*) provides a better match compared to on-site observations (Figure 9d). Further adjustments are adopted by introducing rigid continuous beams (bond beams) along each partition wall, partially restricting the displacement of interior URM walls and providing limited diaphragm action (*Config#5*). Finally, a very similar collapse mechanism is noted when the bond beams are replaced with a rigid floor slab (*Config#6*), as shown in Figure 9e. The results indicate that the localized overturning mechanism at the upper storey can be attributed to a lack of orthogonal load-bearing walls or a roof structure that can provide diaphragm action in the second storey of the building.

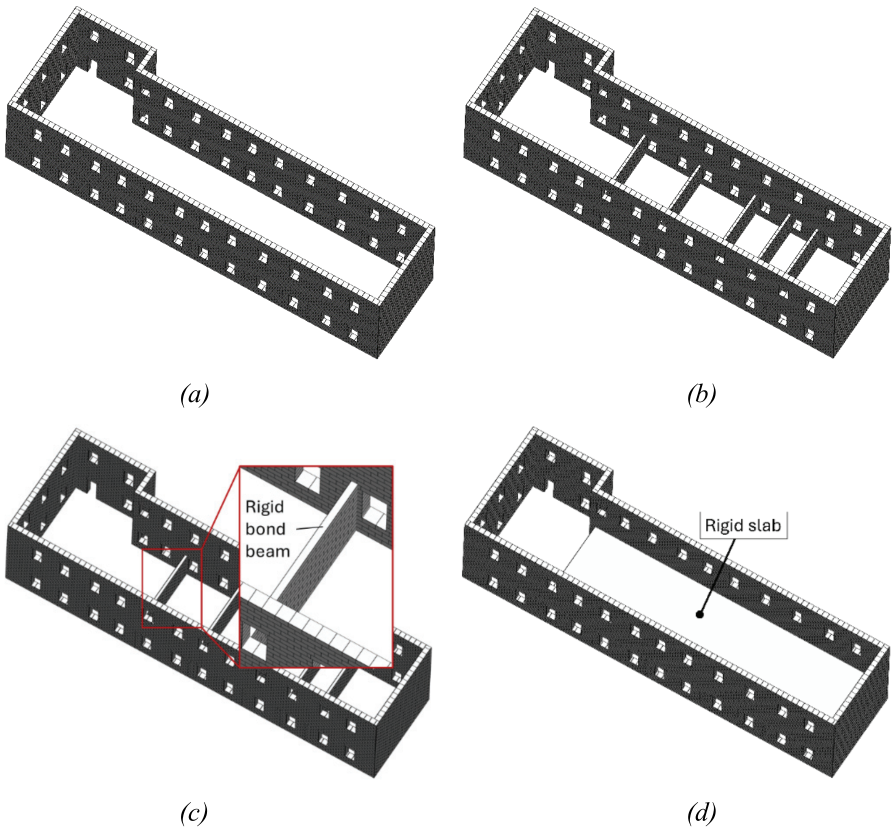

Figure 8 - Proposed structural configurations for the Mithatpaşa Building: (a) no internal walls, (b) addition of the interior walls, (c) implementation of continuous rigid beam between two façades, and (d) interior wall + rigid slab.

In Figure 10, the accelerations required to cause collapse according to the nonlinear quasi-static analyses are provided for each structural configuration. The results underline the positive influence of the adopted bond beams and slabs on the lateral load carrying capacity of the URM buildings, denoted in *Config#5* and *Config#6*, respectively. Interestingly, the interior orthogonal walls in *Config#4* also have a similar effect on the response. Conversely, the lack of either a stiff diaphragm or orthogonal walls yields considerably lower capacity, as depicted in Figure 10 (*Config#1*). The remaining case studies (from *Config#2* to *Config#4*) provide seismic resistance bounded by *Config#1* and *Config#5*. According to Bozyigit et al. [28], the peak ground acceleration in the N-S direction of the nearest seismograph (3115) for the 6th of February Pazarcik earthquake was 0.33*g;* all the examined configurations would be expected to fail according to the analyses. However, the analyses provide more insight into how the failures may have occurred. If combined with detailed material characterization, they can produce more definitive estimates of collapse accelerations. This has not been attempted in this study, which is focused on developing more qualitative forensic understanding of behavior.

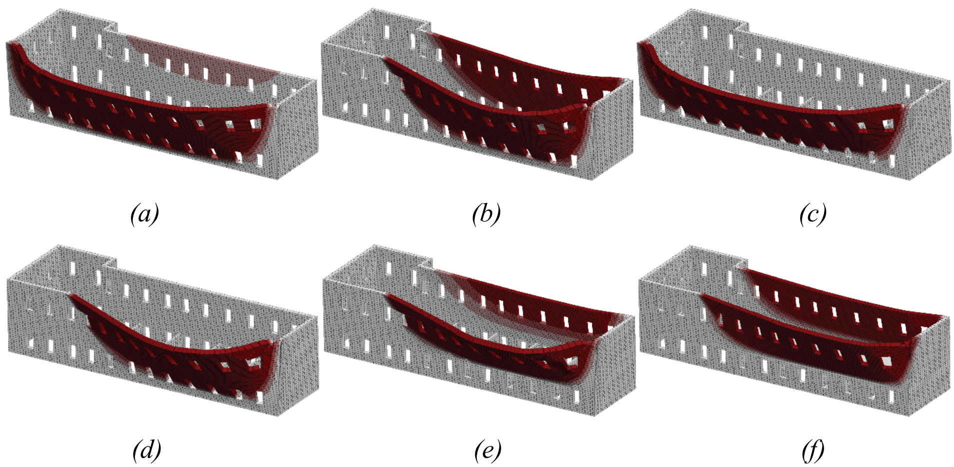

Figure 9 - Predicted collapse mechanism of Mithatpaşa building considering different structural configurations: (a) ***Config#1****: No internal walls, (b)* ***Config#2****: No internal walls – extruded portion fixed, (c)* ***Config#3****: Addition of the internal walls, (d)* ***Config#4****: Internal walls – extruded portion fixed, (e)* ***Config#5****: Internal walls with rigid bond beam – extruded portion fixed and (f)* ***Config#6****: Internal walls with rigid slab - extruded portion fixed.*

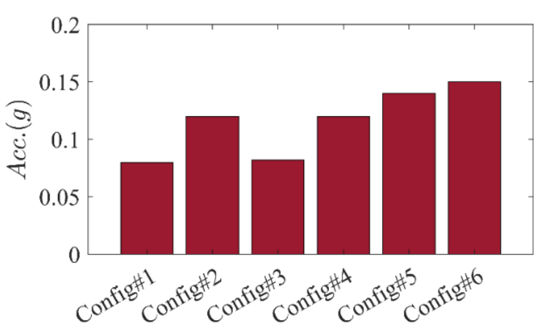

Figure 10 - Lateral acceleration required for collapse in different structural configurations.

4.2. Building #2: Liwan Boutique Hotel

A similar workflow to earlier is adopted for the seismic assessment of the Liwan Boutique Hotel. Once the equilibrium condition is satisfied under self-weight, lateral accelerations are applied along the longitudinal building axis to reproduce the observed out-of-plane failure mechanism in Figure 1b. Two sets of analyses are performed due to uncertainties concerning the roof structure: one set of analyses with and the other without a rigid roof diaphragm resting on the top floor. In addition, due to uncertainties regarding wall morphology and connection between orthogonal walls, several different analysis cases have been investigated to understand the potential influence of these aspects on the response. The analysis cases are summarised in Table 2.

Table 2 - Summary of the characteristics of different analyses used to represent the Liwan Hotel.

Analysis ID	Rigid roof diaphragm	Wall morphology	Connection detailing between orthogonal walls
LH#1	No	Periodic	Vertical joint
LH#2	No	Periodic	Staggered joint
LH#3	No	Nonperiodic with horizontal courses	Staggered joint
LH#4	No	Nonperiodic without horizontal courses (rubble)	Staggered joint
LH#1wR	Yes	Periodic	Vertical joint
LH#2wR	Yes	Nonperiodic	Staggered joint
LH#3wR	Yes	Nonperiodic with horizontal courses	Staggered joint
LH#4wR	Yes	Nonperiodic without horizontal courses (rubble)	Staggered joint

As shown in Figure 11, three wall morphologies are investigated. For the periodic pattern, two cases are considered: one with a vertical corner joint, offering no interlocking between the orthogonal walls (LH#1 and LH#1wR), and the other with a staggered joint linking the two walls (LH#1 and LH#1wR). For the nonperiodic morphologies, a staggered joint is always used. However, it can be visually observed from Figure 11 that the interlocking for the irregular masonry pattern with horizontal courses is likely to be better than the one without the horizontal courses (*e.g.*, the rubble morphology).

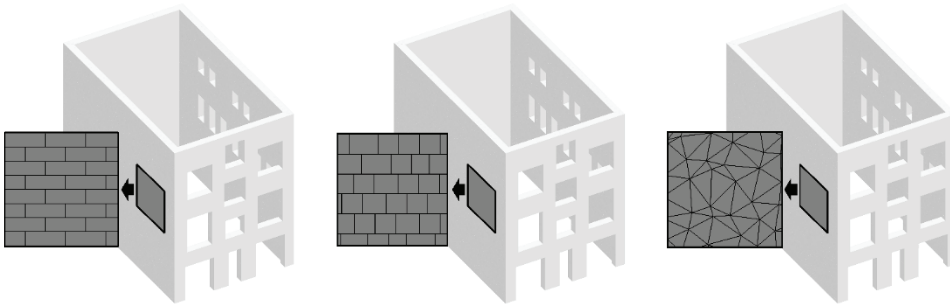

(a) (b) (c)

Figure 11 - The investigated URM construction morphologies: (a) periodic, (b) nonperiodic with horizontal courses and (c) nonperiodic without horizontal courses (rubble).

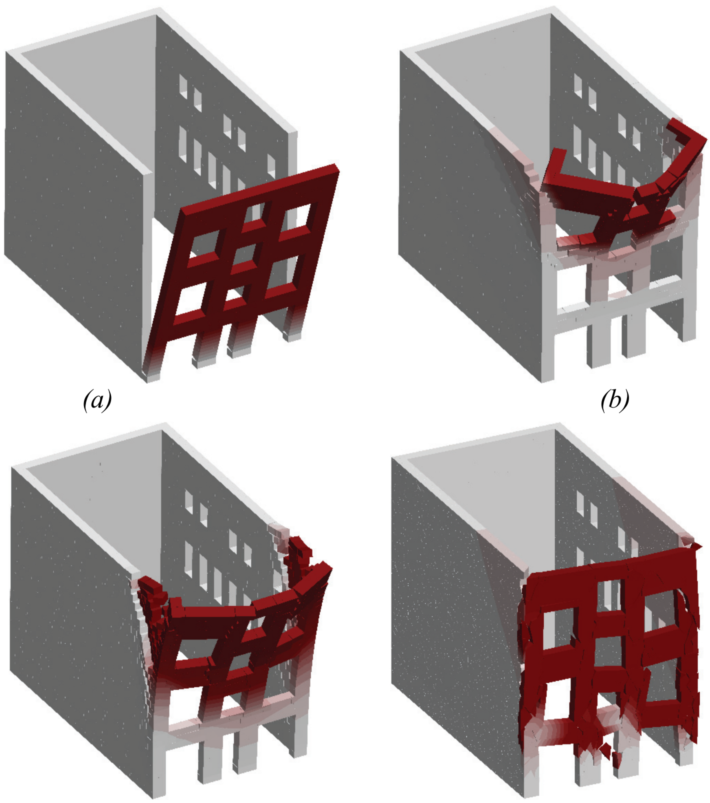

(a) (b)

(c) (d)

Figure 12 - Predicted collapse mechanisms considering different construction morphologies without any horizontal diaphragm: (a) periodic masonry, vertical joint between front façade and orthogonal walls (LH#1), (b) periodic masonry, staggered joint between front façade and orthogonal walls (LH#2), (c) nonperiodic masonry walls (LH#3) and (d) rubble masonry walls (LH#4).

The predicted collapse mechanisms are shown in Figure 12 and Figure 13, for buildings without and with a rigid roof diaphragm, respectively. Given the detachment of the façade from the roof in Figure 1b, the roof is not considered at first. In Figure 12a, the failure mechanism of (LH#1) is presented where only the front façade overturns. In comparison, the same running bond construction with the addition of staggered joints at the intersection of the orthogonal walls (LH#2) demonstrates a partial façade collapse mechanism localized at the upper floors of the building (Figure 12b). Figure 12c and Figure 12d show the results of nonperiodic constructions: (LH#3) describes a building with horizontal courses, and (LH#4) a rubble construction without horizontal courses. The results show that LH#3 involves a failure mechanism involving the longitudinal walls, with diffuse joint openings. In contrast, the rubble morphology in LH#4 fails by masonry disaggregation prior to the formation of a local failure mechanism.

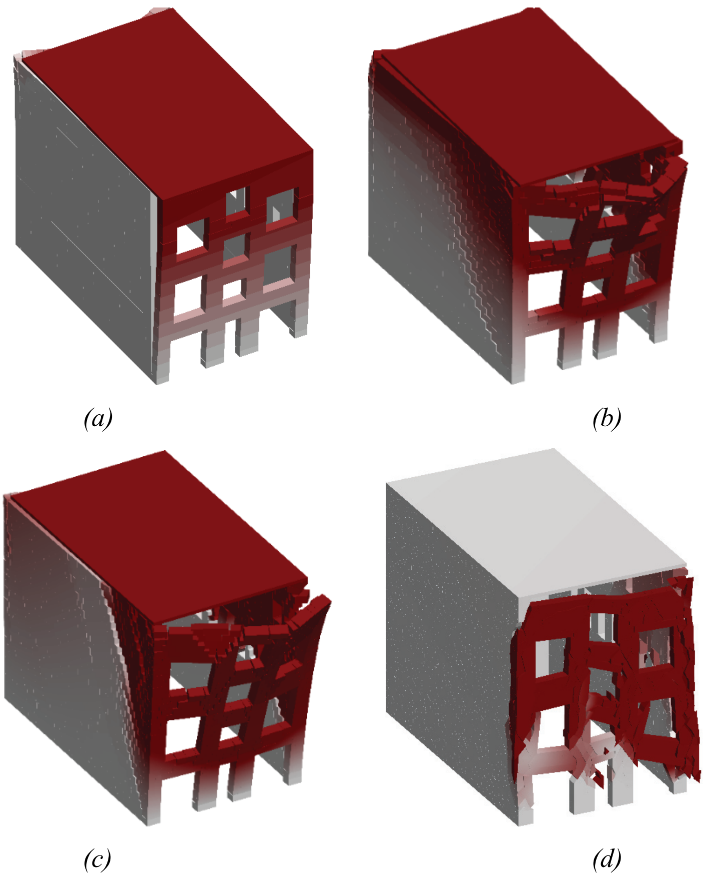

Figure 13 - Predicted collapse mechanisms considering different construction morphologies and considering a rigid roof diaphragm: (a) periodic masonry, vertical joint between front façade and orthogonal walls (LH#1), (b) periodic masonry, staggered joint between front façade and orthogonal walls (LH#2), (c) nonperiodic masonry walls (LH#3) and (d) rubble masonry walls (LH#4).

Only frictional resistance is considered in the computational model to replicate the poor bonding between the roof and the supporting walls. In this case LH1wR (Figure 13a) yields a one-way bending behavior with a total separation of the front façade from the rest of the building due to the partial dead load of the roof. This does not match the partially collapsed state of the building in Figure 1b, where the failure mechanism also involves the side walls. LH#2wR considers good connections between orthogonal walls and extends the failure mechanism to the longitudinal walls (Figure 13b). The results highlight the critical influence of connection details. However, this still does not capture the failure mode observed in the building. The nonperiodic masonry cases (LH#3wR and LH#4wR) are also investigated. The results show that LH#3wR experiences significant in-plane deformations near the centre of the western façade (indicating increased participation of the orthogonal wall in the collapse mechanism with respect to Figure 12c), similar to LH#2wR, while the rubble masonry texture again fails by disaggregation, as shown in Figure 13d. The disaggregation response is not significantly influenced by the additional frictional restraints provided by the roof structure; the poor construction quality dictates the disaggregation failure prior to the formation of any other local response mechanisms.

Finally, Figure 14 shows the lateral collapse acceleration obtained from the nonlinear quasi-static analysis for each wall configuration and their associated corner average staggering ratio (M_l). Note that this ratio is computed at the intersection between the front façade and perpendicular walls since the failure is governed by the detachment of the front façade and, eventually, the vertical overturning mechanism. The results indicate that the lowest seismic multiplier is obtained for the rubble masonry building (LH#4 and LH#4wR), which has experienced a wall disaggregation failure. A slight increase in accelerations is noticed for the failure of the structure where no connection is present between the front façade and side walls (LH#1 and LH#1wR). However, both configurations underline the vulnerability of the buildings to poor corner detailing. The highest seismic capacity is obtained for the running bond pattern with and without roof diaphragm (LH#2 and LH#2wR), demonstrating the positive influence of construction morphology. Nonperiodic wall constructions with horizontal courses (LH#3 and LH#3wR) indicate an intermediate seismic capacity. The positive influence of the roof diaphragm can be associated with notable increases in seismic capacity for all cases except LH#4 and LH#4wR.

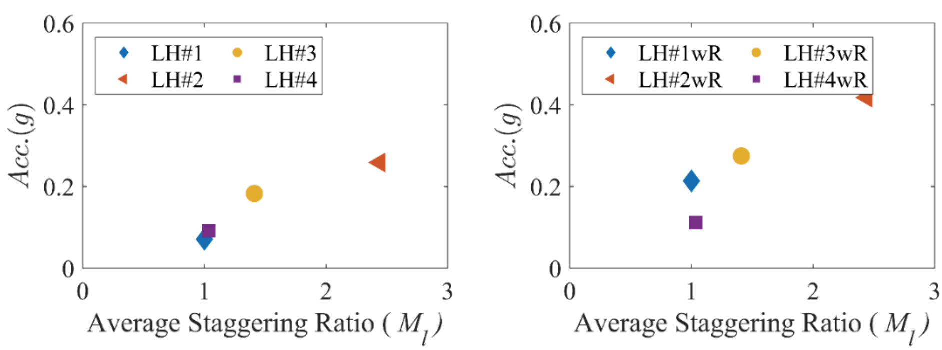

(a) *(b)*

Figure 14 - Lateral accelerations associated with predicted collapse mechanism and masonry construction morphology: (a) without a rigid roof and (b) including a rigid roof.

According to Bozyigit et al. [28], the peak ground acceleration in the E-W direction of the nearest seismograph (3132) for the 6th of February Pazarcik earthquake was 0.54*g;* all the examined configurations would be expected to fail according to the analyses. However, like the case study before, the analyses provide more insight into how the failures may have occurred.

5. CONCLUSIONS

This research conducts a forensic investigation on the seismic response of two buildings that suffered partial collapses during the Kahramanmaraş Earthquakes in 2023. The out-of-plane collapse mechanisms observed in both buildings are predicted using a new reverse engineering approach benefitting from remote sensing data and automated model generation algorithms. Several conclusions can be drawn from the conducted analyses:

- Due to the challenges of acquiring geometrical information after a seismic event, creating digital representations of damaged or partially collapsed unreinforced masonry structures can be complicated. The presented case studies demonstrate the effectiveness of compiling geometric information from multiple vision-based data sources to obtain geometrical measurements that can be employed in computational modeling.
- The proposed automatic block generation algorithms generate periodic and nonperiodic block patterns representing various masonry construction morphologies. The adopted approach significantly improves efficiency compared to manual block-generation strategies and facilitates iterative investigation of discrete element models for forensic purposes.
- It is demonstrated that the proposed discontinuum-based modeling strategy, which considers different boundary conditions and floor structures, captures the post-earthquake condition of the Mithatpaşa Building. This approach provides insights into the building's *as-is* condition, notably by highlighting how the lack of interior walls and roof diaphragm action played a key role in the collapse of the second storey of the building.
- The analysis of the second case study building, the Liwan Boutique Hotel, demonstrated the influence of wall morphology (in particular, interlocking between orthogonal walls) on the overall behavior of the structure. Despite a lack of data, analyses of different wall morphologies (generated using automated or semi-automated tools) highlight how deficiencies in corner detailing and poor morphology may have contributed to the observed failure.

Overall, the findings highlight the need for an automated framework capable of representing diverse masonry textures and patterns to improve the reliability of structural assessments. This is especially critical for rubble buildings with poor quality construction, which may experience local disaggregation failures that can cascade to premature global failures. The implemented block-generation algorithm will be extended in future studies to more realistic rubble geometries, informed by the automatic visual characterization of masonry quality index parameters. Finally, incremental dynamic analyses are suggested in future studies to develop more insight into the seismic response of the analyzed buildings.

References

[1] Roca P, Cervera M, Gariup G, Pelà L (2010) Structural analysis of masonry historical constructions. Classical and advanced approaches. Arch Comput Methods Eng 17:299–325. https://doi.org/10.1007/s11831-010-9046-1

[2] Lourenço PB, Rots JG, Blaauwendraad J (1998) Continuum model for masonry: Parameter estimation and validation. J Struct Eng 124:642–652. https://doi.org/10.1061/(ASCE)0733-9445(1998)124:6(642)

[3] Funari MF, Spadea S, Lonetti P, et al (2020) Visual programming for structural assessment of out-of-plane mechanisms in historic masonry structures. J Build Eng 31:101425. https://doi.org/10.1016/j.jobe.2020.101425

[4] Funari MF, Hajjat AE, Masciotta MG, et al (2021) A parametric scan-to-FEM framework for the digital twin generation of historic masonry structures. Sustain 13:11088. https://doi.org/10.3390/su131911088

[5] Saloustros S, Pelà L, Contrafatto FR, et al (2019) Analytical Derivation of Seismic Fragility Curves for Historical Masonry Structures Based on Stochastic Analysis of Uncertain Material Parameters. Int J Archit Herit 13:1142–1164. https://doi.org/10.1080/15583058.2019.1638992

[6] Lourenço PB, Rots JG (1997) Multisurface interface model for analysis of masonry structures. J Eng Mech 123:660–668

[7] Foti D, Vacca V, Facchini I (2018) DEM modeling and experimental analysis of the static behavior of a dry-joints masonry cross vaults. Constr Build Mater 170:111–120. https://doi.org/10.1016/j.conbuildmat.2018.02.202

[8] Pulatsu B, Erdogmus E, Lourenço PB, et al (2020) Discontinuum analysis of the fracture mechanism in masonry prisms and wallettes via discrete element method. Meccanica 55:505–523. https://doi.org/10.1007/s11012-020-01133-1

[9] Gonen S, Pulatsu B, Erdogmus E, et al (2021) Quasi-static nonlinear seismic assessment of a fourth century A.D. Roman Aqueduct in Istanbul, Turkey. Heritage 4:401–421. https://doi.org/10.3390/heritage4010025 https://doi.org/10.3390/infrastructures7030031

[10] Pulatsu B, Tuncay K (2024) Computational Modeling of Damage Progression in Unreinforced Masonry Walls via DEM. Turkish J Civ Eng 35:. https://doi.org/10.18400/tjce.1323977

[11] Malomo D, Pulatsu B (2024) Discontinuum models for the structural and seismic assessment of unreinforced masonry structures: a critical appraisal. Structures 62:106108. https://doi.org/10.1016/j.istruc.2024.106108

[12] Griesbach P, Wilson R, Karakus B, Pulatsu B (2023) Transferring vision-based data to discontinuum analysis for the assessment of URM walls. Eur J Environ Civ Eng 0:1–16. https://doi.org/10.1080/19648189.2023.2254376

[13] Loverdos D, Sarhosis V (2024) Pixel-level block classification and crack detection from 3D reconstruction models of masonry structures using convolutional neural networks. Eng Struct 310:118113. https://doi.org/10.1016/j.engstruct.2024.118113

[14] Milani G, Esquivel YW, Lourenço PB, et al (2013) Characterization of the response of quasi-periodic masonry: Geometrical investigation, homogenization and application to the Guimarães castle, Portugal. Eng Struct 56:621–641. https://doi.org/10.1016/j.engstruct.2013.05.040

[15] Loverdos D, Sarhosis V (2023) Image2DEM: A geometrical digital twin generator for the detailed structural analysis of existing masonry infrastructure stock. SoftwareX 22:101323. https://doi.org/10.1016/j.softx.2023.101323

[16] Garbioglu Ö (2017) Tanzimat'tan Cumhuriyet'e Hatay'daki Kamu Yapilari. Mimar Sinan Güzel Sanatlar Üniversitesi

[17] Cundall PA (1971) A computer model for simulating progressive, large-scale movements in blocky rock systems. In: The International Symposium on Rock Mechanics. Nancy, pp 47–65

[18] Cundall PA (1988) Formulation of a Three-dimensional Disctinct Element Model - Part I. A Scheme to Detect and Represent Contacts in a System Composed of Many Polyhedral Blocks. Int J Rock Mech Min Sci Geomech 25:107–116

[19] Hart R, Cundall PA, Lemos J V. (1988) Formulation of a three-dimensional distinct element model - Part II. Mechanical calculations for Motion and Interaction of a System Composed of Many Polyhedral Blocks. Int J Rock Mech Min Sci Geomech 25:117–125

[20] Pulatsu B, Erdogmus E, Lourenço PB, et al (2020) Simulation of the in-plane structural behavior of unreinforced masonry walls and buildings using DEM. Structures 27:2274–2287. https://doi.org/10.1016/j.istruc.2020.08.026

[21] Pulatsu B (2023) Coupled elasto-softening contact models in DEM to predict the in-plane response of masonry walls. Comput Part Mech 10:1759–1770. https://doi.org/10.1007/s40571-023-00586-x

[22] Itasca Consulting Group Inc. (2013) 3DEC Three Dimensional Distinct Element Code

[23] Cundall PA, C. D (2017) Dynamic relaxation applied to continuum and discontinuum numerical models in geomechanics, 1st Editio. CRC Press, Boca Raton, FL

[24] Pirchio D, Walsh KQ, Kerr E, et al (2021) Integrated framework to structurally model unreinforced masonry Italian medieval churches from photogrammetry to finite element model analysis through heritage building information modeling. Eng Struct 241:112439. https://doi.org/10.1016/j.engstruct.2021.112439

[25] Crespi P, Franchi A, Ronca P, et al (2015) From BIM to FEM: the analysis of an historical masonry building. Build Inf Model Des Constr Oper 1:581–592. https://doi.org/10.2495/bim150471

[26] Milani G, Esquivel YW, Lourenço PB, et al (2013) Characterization of the response of quasi-periodic masonry: Geometrical investigation, homogenization and application to the Guimarães castle, Portugal. Eng Struct 56:621–641. https://doi.org/10.1016/j.engstruct.2013.05.040

[27] Loverdos D, Sarhosis V, Adamopoulos E, Drougkas A (2021) An innovative image processing-based framework for the numerical modeling of cracked masonry structures. Autom Constr 125:103633. https://doi.org/10.1016/j.autcon.2021.103633

[28] Bozyigit B, Ozdemir A, Donmez K, et al (2024) Damage to monumental masonry buildings in Hatay and Osmaniye following the 2023 Turkey earthquake sequence: The role of wall geometry, construction quality, and material properties. Earthq Spectra. https://doi.org/10.1177/87552930241247031

[29] Mijic N, Sestic M, Koljancic M (2017) CAD—GIS BIM Integration—Case Study of Banja Luka City Center. In: Hadzikadic M, Avdakovic S (eds) Lecture Notes in Networks and Systems 3. Spring International Publishing, pp 267–281

[30] Ferrante A, Loverdos D, Clementi F, et al (2021) Discontinuous approaches for nonlinear dynamic analyses of an ancient masonry tower. Eng Struct 230:111626. https://doi.org/10.1016/j.engstruct.2020.111626

[31] Mishra M, Lourenço PB (2024) Artificial intelligence-assisted visual inspection for cultural heritage: State-of-the-art review. J Cult Herit 66:536–550. https://doi.org/10.1016/j.culher.2024.01.005

[32] Borri A, Corradi M, De Maria A (2020) The Failure of Masonry Walls by Disaggregation and the Masonry Quality Index. Heritage 3:1162–1198. https://doi.org/10.3390/heritage3040065

[33] Borri A, Corradi M, Castori G (2015) A method for the analysis and classification of historic masonry. Bull Earthq Eng 2647–2665. https://doi.org/10.1007/s10518-015-9731-4

[34] Wilson R, Pouragha M, Acikgoz S, Pulatsu, B (2025) A DEM-based computational modelling framework to investigate fracture processes in clay brick and masonry composite. Computational Particle Mechanics. (Accepted)

[35] Erdogmus E, Pulatsu B, Gaggioli A, Hoff M (2021) Reverse Engineering a Fully Collapsed Ancient Roman Temple through Geoarchaeology and DEM. Int J Archit Herit 15:1795–1815. https://doi.org/10.1080/15583058.2020.1728593

[36] Alexakis H, Makris N (2017) Hinging Mechanisms of Masonry Single-Nave Barrel Vaults Subjected to Lateral and Gravity Loads. J Struct Eng 143:4017026. https://doi.org/10.1061/(asce)st.1943-541x.0001762

[37] Lourenço PB, Gaetani A (2022) Recommended properties for advanced numerical analysis. In: Finite Element Analysis for Building Assessment. Routledge, New York, pp 209–320